Hindawi
Advances in Civil Engineering
Volume 2018, Article ID 4186943, 13 pages
https://doi.org/10.1155/2018/4186943

Research Article

Testing the Explosion Resistance and Energy Absorption of a Polyurethane-Foamed Aluminum Composite Structure

Zhang Yong, Xue Zheng-yu, Lin Zhen-rong, Lu Yu-song, and Wang Xiao-hui

Key Protective Materials Laboratory of the Military 2110 Project, Department of Airport Engineering, Airforce Service College, Xuzhou 221000, Jiangsu, China

Correspondence should be addressed to Zhang Yong; freebirdzy1980@163.com

Received 8 May 2018; Revised 5 August 2018; Accepted 12 September 2018; Published 25 October 2018

Guest Editor: Yanchao Shi

Concrete structures can suffer damage from the shock waves caused by explosions. However, the damage can be mitigated in practice by increasing the size of the energy-absorbing interlayers to improve the antiknock performance of the concrete. The aim of this paper is to investigate the energy-absorbing capability of a composite structure of polyurethane-foamed aluminum and concrete. The composite structure consisted of C60 concrete with foamed aluminum or polyurethane-foamed aluminum as a sandwich material. The thickness of the interlayers and the relative amounts of the different materials in the structure were the variables that were adjusted from test to test. To capture data related to the explosion, the structure was instrumented with pressure, acceleration, strain gauge, and displacement sensors. The efficacy of this structure was validated by way of surface contact explosions using 0.5 kg of TNT. By appropriately positioning the explosives in each test, the related parameters in the explosions, including the stress, displacement, acceleration, and strain, were recorded. The results of the tests indicated that the energy-absorbing capability of the polyurethane-foamed aluminum was significantly higher than that of the foamed aluminum, and the thickness of the energy-absorbing layer had a great impact on the energy absorption effect.

1. Introduction

In wars, terrorist attacks, and other events, concrete structures may be damaged by shock waves from explosions. Thus, it has become important for researchers to determine how to increase the antiknock performance of concrete structures. The explosion resistance performance of two groups of high-strength reinforced concrete (RC) slabs versus common RC slabs was studied experimentally by Lu et al. [1] as part of an exploration into the failure mechanisms and the development and distribution of cracks in concrete. The results indicate that the adoption of HHT 600 high-strength steel bars can effectively reduce the development of cracks and enhance the explosion resistance performance of RC slabs. Zhai et al. [2] investigated the performance of RC structures subjected to blast loading after being exposed to fire. The experimental and numerical results showed that RC beams after being exposed to fire suffered greater blast-induced damage than those that were not exposed to fire. Zong et al. [3] investigated the dynamic response characteristics, damage modes, and failure mechanisms of reinforced concrete (RC) piers under blast loading and near-field and contact explosion tests while considering different cross-sectional shapes, the slenderness ratio, the type of concrete, the form of stirrup, and the parameters related to the axial compression ratio in order to determine a suitable fitting formula. Chen et al. [4, 5] conducted an experimental study of the combined effects of a high temperature and high strain rate on normal concrete materials and provided a new empirical model to describe the dynamic increase in the strength factor and the secant elastic modulus of concrete at elevated temperatures. In recent years, interlayer-type structures that incorporate new energy-absorbing layers in the form of foamed metal have received significant research and development attention. Shen et al. [6] applied a blast load via an explosion to a curved laminboard with an aluminum panel and foamed aluminum core to study its dynamic response and found that

the curved laminboard could absorb more explosive energy than a solid board and an interlayer plate of an equal weight. This further demonstrated the excellent properties of foamed aluminum in resisting explosion shock. Merrett et al. [7] used foamed aluminum when conducting explosion tests to study the wave surface effect under shock wave compression. Yun et al. [8] analyzed the energy-absorbing and -buffering functions of foamed aluminum materials in the interlayer of a steel plate and found that reinforcing the concrete wall by way of a sacrificial layer of foamed aluminum could dramatically reduce the influence of the bursting pressure. Polyurethane is a foam material with a small specific gravity, low price, and good workability. Due to its excellent energy and shock-absorbing capabilities, it has been widely used for protection in the packaging of fragile goods, construction of protective layers, inner filling of relevant structures, and national defense applications [9–11]. Zhang et al. [12] analyzed the static mechanical properties of the foamed aluminum-polyurethane composite material. Xie et al. and Zhang et al. studied the kinetic performance of the polyurethane-foamed aluminum composite material via relevant experiments [13–15].

In this study, polyurethane foam was used in a perforated foamed aluminum plate to fabricate the advanced composite material called polyurethane-foamed aluminum. This combination enhanced the energy-absorbing capability of foamed aluminum. The focus of the current study is to investigate the explosion resistance and energy absorption characteristics of a concrete plate composite structure when polyurethane-foamed aluminum is used as the energy-absorbing interlayer.

2. Test Design

The structures designed for the explosion tests included C60 concrete with thicknesses of 100 and 220 mm. A 100 mm thick overburden layer was applied to the concrete, and the surface of this layer was subjected to a contact explosion of 0.5 kg of TNT. In the test, foamed aluminum and polyurethane-foamed aluminum plates were selected as the interlayer materials. The thicknesses of the interlayer material and different combinations of materials were used as variables. Five tests were designed to study the explosion resistance capability of the polyurethane-foamed aluminum.

2.1. Preparation of the Test Specimens

2.1.1. Preparation of the Polyurethane-Foamed Aluminum. As shown in Figure 1, polyurethane-foamed aluminum was prepared by mixing and foaming the black (toluene diisocyanate: PM200) and white (polyether ternary alcohol: N303, hydroxyl value: 470 mg KOH/g) ingredients of polyurethane.

The parameters of the open-cell aluminum foam produced by Shanghai Zhonghui Foam Aluminum Co., Ltd., are shown in Table 1.

First, a certain amount of black material was added to the foamed aluminum plate and spread evenly over the plate until it was absorbed. Then, the white material was added according to a mass ratio of 1 : 1 so as to mix it with the black material and cause them to react and foam. A purpose-built generation vessel was pressurized to force the produced polyurethane foam into the voids of the foamed aluminum plate.

The weight of the polyurethane-foamed aluminum plate was much higher than that of the foamed aluminum plate. When analyzed, the weight of the polyurethane-foamed aluminum plate increased from 73.79% to 89.29%. This was because the amount of polyurethane had significantly increased the weight. The result was a fairly ideal composite material that was suitable for use in the subsequent explosion resistance and energy absorption tests.

2.1.2. Preparation of the Concrete. Table 2 shows the mixture ratio of the concrete.

Additional details are as follows:

(i) The cement was P.O. 52.5 ordinary Portland cement

(ii) The pebbles should meet the continuous grading requirement for a maximum particle size of 20 mm

(iii) Silica fume produced in Xuzhou was used

(iv) Grade II coal ash was used

(v) A polycarboxylate-type high-efficiency slushing agent was used

The concrete plate in this test was fabricated by manual mixing. The raw material was prepared as per the relevant mix proportions, and the concrete was mixed as per the standard procedure. Once mixed, the concrete was poured into a mold and vibrated. Finally, the finished concrete sample was cured for 28 d in a suitable environment before the explosion tests were conducted. The in-progress concrete plates are shown in Figure 2.

2.2. Test Setups. During the tests, concrete composite boards with polyurethane-foamed aluminum as the energy-absorbing interlayer were utilized to study the destructive effects of an explosive load of 0.5 kg TNT, as shown in Figure 3. Five different combinations of the material were prepared, as shown in Figure 4.

The five tests varied according to the interlayer material type, thickness, and combination of materials. The observed phenomena and the sensor data captured during the explosions were used to analyze the explosion resistance performance of the polyurethane-foamed aluminum. In the second and third tests, the polyurethane-foamed aluminum was compared with foamed aluminum in terms of the explosion resistance performance. Then, in the fourth and fifth tests, the effects of the interlayer material thickness and the combination of materials on the explosion resistance performance of the structure were studied. By comparing the results of the latter tests (Tests 2, 3, 4, and 5) with the results of the first test (Test 1), the differences between the explosion resistance performance of the single-layer concrete structure and that of the composite structures were studied.

(a) (b)

Figure 1: Preparation of the polyurethane-foamed aluminum.

Table 1: Parameters of the open-cell aluminum foam.

Aperture	Porosity	Hole rate	Bulk density	Compressive strength σ_c	Bending strength σ_w	Tensile strength σ_b
1.66 mm	68–78%	90–95%	0.60–0.85 g/cm^3	8.61 MPa	8.06 MPa	3.41 MPa

Table 2: Mixture ratios of the concrete (kg/m^3).

Water	Cement	Silicon	Fly ash	Sand	Stone	Water-reducing agent
150	370	50	80	595	1155	9

Figure 2: Concrete preparation.

Figure 3: 0.5 kg TNT.

3. Field Explosion Test

As shown in Figure 5, a 1 m high steel structure was purposely built for this test. The top of the structure matched the size of the concrete samples so that the bottom of the test specimens was suspended in air. The steel structure was assembled in an open field, and measurement points were chosen for the concrete plate and the interlayer layer that were relatively close to the steel structure. Electric circuit adapters to facilitate the measurements were placed on the steel structure. After the measuring points were arranged, the concrete and interlayer plates were stacked on and attached to the bracket, and then the top of the upper layer of concrete was covered by dirt.

Due to the large range of an explosive shock wave, the data transmission wires near the center of the explosion were installed in a steel conduit to protect them from damage. For the same reason, the data acquisition system was assembled in a shelter 20 m away from the center of the explosion (Figure 5(b)). The measuring points on the test structure were transmitted via wire to the shelter to prevent effects of the explosion shock wave on the data acquisition system.

Five tests were conducted as per the testing program using the five setups shown in Figure 6.

After the test setups were configured, the data acquisition system was enabled and the operation of the sensors at each point was confirmed. Then, all persons around the test field were evacuated before 0.5 kg of the TNT explosive material was placed on the overburden layer and detonated, as shown in Figure 7.

In the test, the parameters related to the explosion damage, such as the pressure, displacement, acceleration, and strain, were recorded via the measurement points configured in each test. The sensors used at the measurement points are shown in Figure 8.

All of the measurement points were located under the powder charging points. The pressure- and acceleration-measuring points were set on the lower surface of each

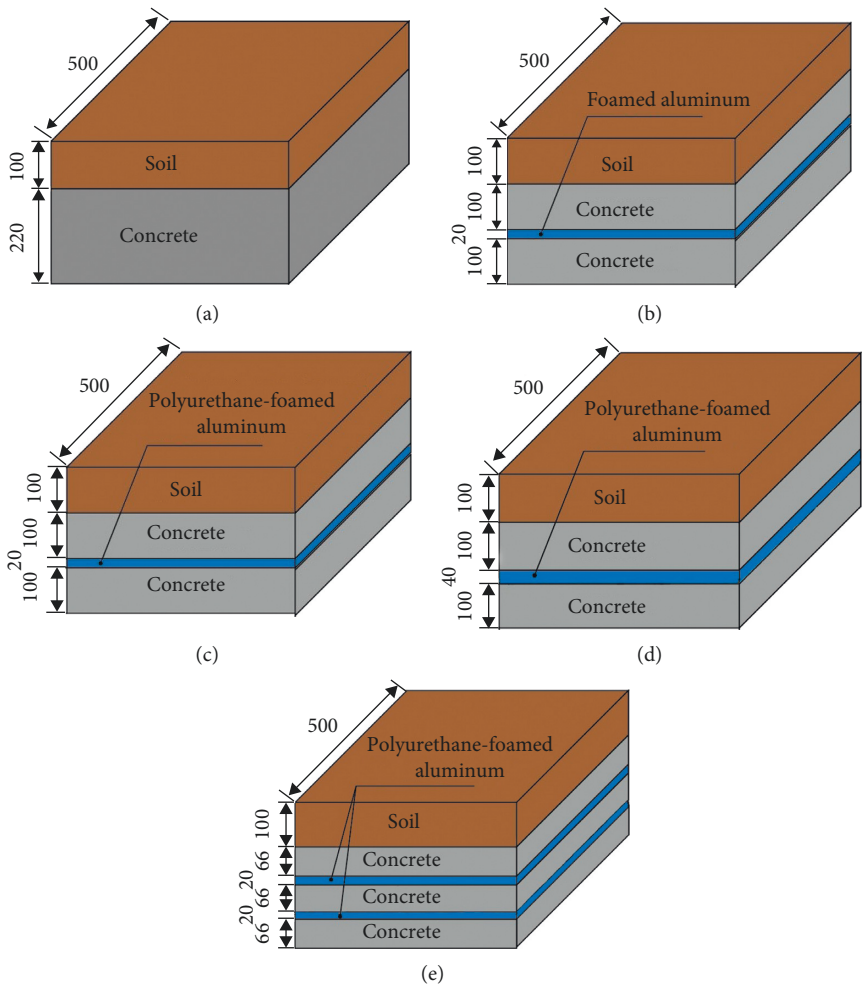

Figure 4: Different test combinations. (a) Test 1. (b) Test 2. (c) Test 3. (d) Test 4. (e) Test 5.

(a) (b)

Figure 5: Test site layout.

intermediate layer, and one displacement point was set on the lower surface of the structure. As no displacement- and velocity-measuring points were placed at the other locations, the displacement and velocity were derived from the acceleration.

In Test 1, there was no measuring point on the testing plate. However, Tests 2, 3, and 4 employed identical arrangements of testing points. For the first layer (concrete plate), a pressure sensor (i.e., overpressure measurement point) was mounted at the center of the lower surface and a second sensor was placed 100 mm away from the center. One acceleration sensor was mounted at a point 50 mm away from the center of the lower surface. For the second layer (either a foamed aluminum plate or

Figure 6: Experimental test setups. (a) Test 1. (b) Tests 2 and 3. (c) Test 4. (d) Test 5.

Figure 7: Explosion.

a polyurethane-foamed aluminum plate), strain gauges were applied after the surface of the concrete was prepared by rubbing. For the third layer (concrete plate), one pressure sensor was mounted at the center of the lower surface and another at a point 100 mm away from the center. In addition, one displacement sensor was mounted on one side (50 mm away from the center) of the lower surface, and one acceleration sensor was mounted on the other side. The arrangement of the sensors in Tests 2, 3, and 4 is shown in Figure 9.

In Test 5, for the first layer (concrete plate), one pressure sensor was mounted at the center of the lower surface and another at a point 100 mm away from the center. For the third layer (concrete plate), one pressure sensor was mounted at the center of the lower surface and another at a point 100 mm away from the center. For the fifth layer (concrete plate), one pressure sensor was mounted at the center of the lower surface and at a point 100 mm away from the center. In addition, one displacement sensor was mounted on one side (50 mm away from the center) of the lower surface, and one acceleration sensor was mounted on the other side. The arrangement of the sensors in Test 5 is shown in Figure 10.

Because this explosion test was performed on a composite material plate and the concrete had a high strength after curing and molding, it was difficult to determine suitable measurement points at which to place the sensors as per the plan and relevant requirements. For this reason, the decision was made to mount the sensors at key points while the concrete was poured. To facilitate this, the acceleration sensor that was placed inside the concrete plate was waterproofed to protect it while the concrete was being poured into the mold. The acceleration sensor in the bottom concrete plate was placed prior to the explosion test. The placement of these sensors is shown in Figure 11.

To ensure there was sufficient space for setting the pressure measurement points while the concrete was being poured, bamboo tubes of an appropriate size were inserted into the concrete.

In this experiment, the data acquisition system consisted of a YE5853B charge amplifier, MSO 3014 oscilloscope, and CS dynamic resistance strain gauge along with a National Instruments NI 9215 data acquisition module. The data were input to a computer via the universal serial bus (USB) interface, and the data collection and reduction

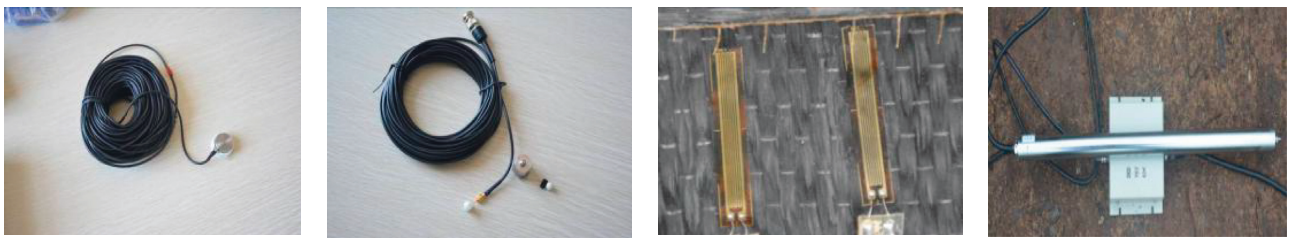

(a) (b) (c) (d)

Figure 8: Types of sensors used in the tests. (a) Pressure sensor. (b) Acceleration sensor. (c) Strain gauge. (d) Displacement sensor.

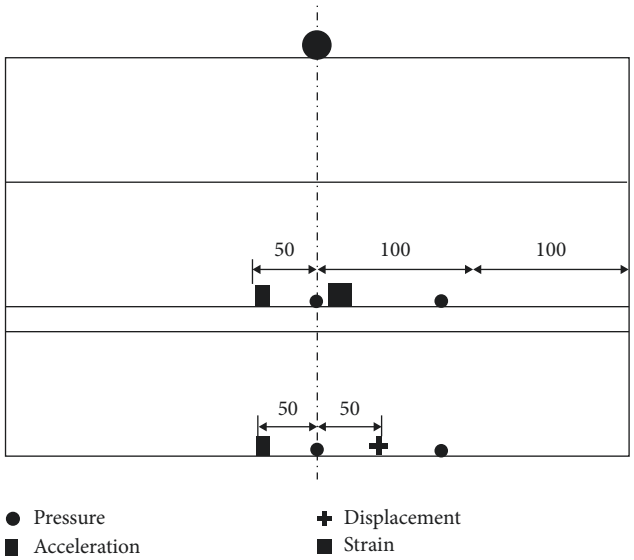

Figure 9: Arrangement of the measurement points in Tests 2, 3, and 4.

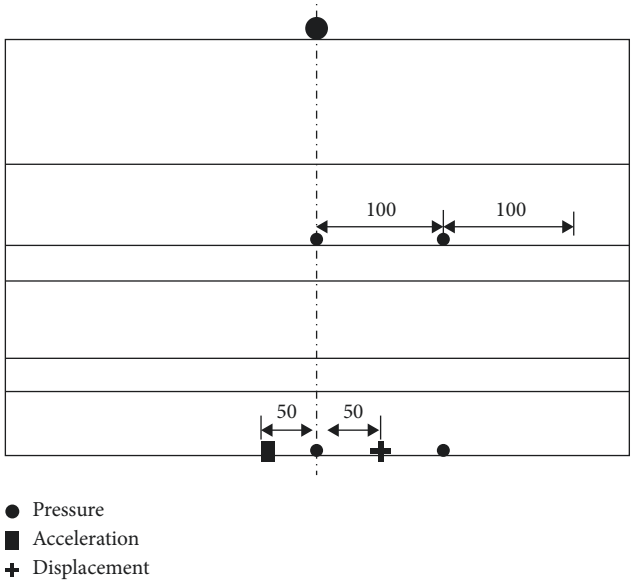

Figure 10: Arrangement of the measurement points in Test 5.

steps employed the self-improved rocket gun dynamic parameter measurement system shown in Figure 12.

4. Results and Analysis

4.1. Analysis of the Test Phenomena. Test 1 employed a 220 mm thick concrete layer. After 0.5 kg of explosive was detonated, the overburden layer was destroyed by the impact force and fragments were strewn around the site. The shock wave also spread downwards to destroy the lower concrete structure. After the explosion, there was a depression on the top of the concrete that extended outward from the center of the concrete plate. The center of the depression was 1-2 cm deep, and the diameter was about 30 cm. Cracks appeared along the sides of the concrete and extended from the upper surface to the bottom. The bottom of the concrete slumped to form pot holes with diameters of 10–15 cm. The damage is shown in Figure 13.

In Tests 2 and 3, foamed aluminum and polyurethane-foamed aluminum were employed as the energy-absorbing interlayers, respectively. In these tests, the upper layer of concrete was severely damaged and fragments were strewn around the site. In addition, the shock wave from the explosion caused compressional deformation of the interlayer material. In the two tests, many cracks appeared in the lower layer of concrete and extended from the top of the bottom plate to the bottom. This is shown in Figure 14.

Compared with Test 1, the bottom sides of the bottom concrete plates, as shown in Figure 15, had better integrity, although the bottom of the concrete in Test 2 was more damaged than that in Test 3. This showed that when polyurethane-foamed aluminum was used as the interlayer of the concrete, it was able to provide more protection to the structure than the foamed aluminum under the same blast load.

As shown in Figure 16, the shock of the explosion caused extensive compressional deformation to the interlayer material in Tests 2 and 3. On the foamed aluminum plate, many cracks appeared in the areas near the depressions. In contrast, the voids in the polyurethane-foamed aluminum plate were filled with polyurethane foam, which allowed the plate to have a certain amount of elasticity. Thus, its compressional deformation was smaller than that of the foamed aluminum plate.

(a) (b)

Figure 11: Sensors buried.

(a) (b)

Figure 12: Rocket gun dynamic parameter measurement system.

(a) (b)

Figure 13: Damage phenomena from Test 1.

In terms of the composite board in Test 4, the thickness of the interlayer material changed from Test 3. After the explosion, the upper concrete plate was not completely fragmented and the backside of the lower concrete plate had a small number of fine cracks. Thus, the integrity of the concrete in this test was better than that in Test 3. Based on this result, the thickness of the polyurethane-foamed aluminum energy-absorbing layer was shown to be an important factor in influencing the explosion resistance capability of the concrete composite plate. These results are shown in Figure 17.

In Test 5, the thicknesses of the layers were changed from those in Test 4 by dividing the 40 mm thick interlayer into two 20 mm layers. Also, the first two layers of concrete were thinner than those in Test 4. The effect of the additional layers intensified the reflection effect of the shock wave between the different media, which caused the first two layers of concrete to be more severely damaged. The bottom of the top layer of concrete had extensive fragmentation and generally poor integrity. In the center of the second layer of concrete from the top, penetrating cracks appeared and the entire plate broke from the middle. Based on the state of the

(a) (b)

Figure 14: Blast damage phenomena from Tests 2 and 3. (a) Damage to the upper layer. (b) Bottom of the lowest plate.

(a) (b)

Figure 15: Damage to the bottom of the concrete in Tests 2 (a) and 3 (b).

(a) (b)

Figure 16: Differences in the damage between the polyurethane-foamed aluminum sandwich (a) and aluminum foam sandwich (b).

surface of the bottom layer of concrete, the bottom layer of concrete in Test 5 retained good integrity and exhibited damage that was much the same as in the same layer in Test 4. These results are shown in Figure 18.

In Test 5, the single layer of polyurethane-foamed aluminum from Test 4 was divided into two layers and placed amid the concrete layers. However, this did not improve the explosion resistance capability of the structure, while its construction became more difficult.

4.2. Analysis of the Pressure and Strain Test Results. The collected data were analyzed with respect to the pressure and strain, and the stress variation of each layer of the material in all tests was observed and analyzed. In this way, the intuitional description of the force analysis in all tests was converted into numerical results. These results are plotted in Figures 19 and 20.

In Figure 19, the measured points were located on the bottom of the upper layer of concrete, and the shock wave

(a) (b)

Figure 17: Complete setup for Test 4 (a) and the damage to the base (b).

(a) (b)

Figure 18: Complete setup for Test 5 (a) and the damage to the back of the base (b).

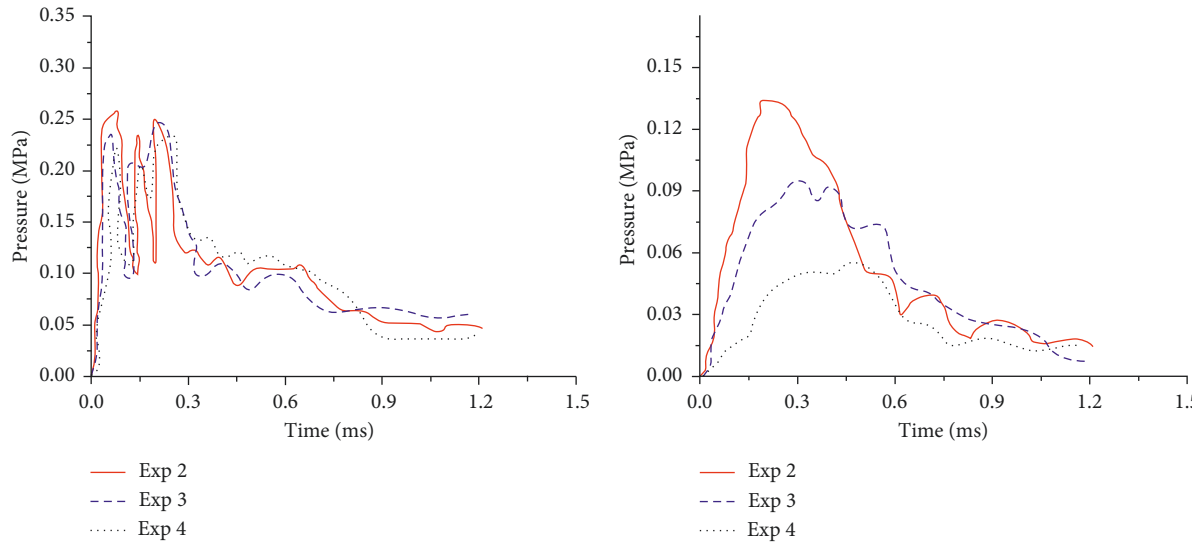

(a) (b)

Figure 19: Pressure-time curves of Tests 2, 3, and 4. (a) Top point. (b) Bottom point.

pressures measured at these locations in Tests 2, 3, and 4 were similar. Thus, the reflected shock waves on the upper layer of concrete were equivalent. From Figure 19, it can be seen that the thickened polyurethane-foamed aluminum in Test 4 had the best attenuation effect on the shock wave pressure, the second best was for the polyurethane-foamed aluminum interlayer used in Test 3, while the attenuation effect of the foamed aluminum interlayer in Test 2 was the

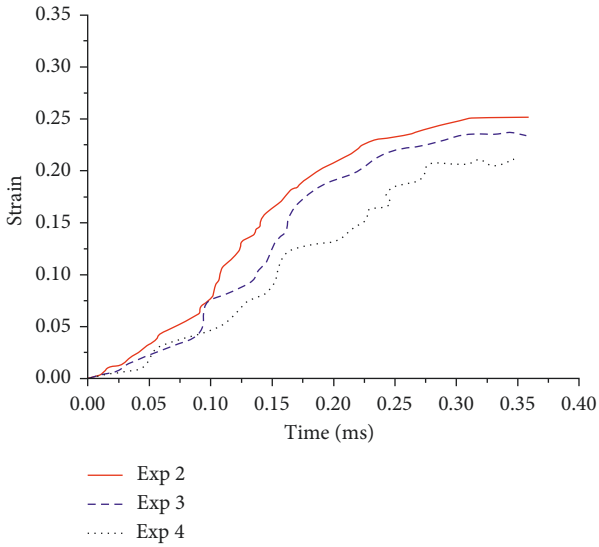

Figure 20: Strain-time curves of the sandwiched materials in Tests 2, 3, and 4.

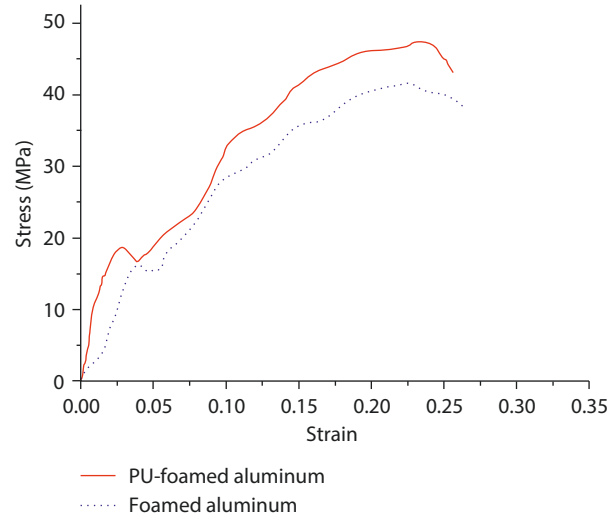

Figure 21: Stress-strain curves for the polyurethane-foamed aluminum and the foamed aluminum.

worst. Because the polyurethane-foamed aluminum in Test 4 was thicker than that in Test 3, this delayed the time for the shock wave to arrive at the bottom layer of concrete. This caused the peak value of the pressure curve in Test 4 to appear later than those of the pressure curves in Tests 2 and 3.

The deformation of the interlayer materials in the different tests that were subjected to shock wave destruction is shown in Figure 20. In Test 2, during deformation, voids in the foamed aluminum were gradually squeezed and compacted. However, as the voids in the polyurethane-foamed aluminum were filled with the polyurethane foam material, the corresponding deformation was less than that in the foamed aluminum material, and the strain displayed in the curve was smaller.

The relationship between the pressure and strain was analyzed to obtain the stress-strain curves of the interlayer materials under explosive conditions. These curves are shown in Figure 21.

4.3. Analysis of the Acceleration Test Results. In this test, the acceleration sensor buried in the concrete was used to measure the acceleration. The associated curves are shown in Figure 22. In Figure 22(a), the peak curve of Test 3 was smaller than that of Test 2. Because the shock resistance of the polyurethane-foamed aluminum interlayer material was superior to that of the foamed aluminum used in Test 2, the bottom concrete in Test 3 deformed slowly after the shock wave went through the interlayer material. In Test 4, because the interlayer material was thicker, it could absorb more energy while resisting the shock wave and therefore better protect the bottom concrete structure. For this reason, the concrete deformation speed in the curve of Test 4 was the slowest. As there was little difference between the two curves in Figure 22(b), it was difficult to compare the deformation speeds of the bottom concrete in Tests 4 and 5. Even so, after the explosions, the bottom concrete in both tests exhibited similar damage.

4.4. Analysis of the Displacement Test Results. The displacement-monitoring points were located on the bottom of the last layer of concrete, which meant that the displacement caused by a shock wave could be measured.

It can be seen in Figure 23 that the displacement values of the bottom concrete in Tests 2, 3, and 4 varied with time and the respective displacements increased gradually. These results demonstrate that the polyurethane-foamed aluminum interlayer provided better explosion resistance to the overall structure than did the foamed aluminum interlayer. However, by adding an equivalent composite layer, increasing the thickness of the polyurethane-foamed aluminum interlayer was found to be an effective way to enhance the explosion resistance capability of the protective structure. The displacement curves of the bottom concrete layers in Tests 4 and 5 were almost equivalent, which indicated that the protective capability of the polyurethane-foamed aluminum interlayer material for the bottom concrete was no different before or after layering.

4.5. Analysis of the Quantity and Efficiency of Energy Absorption. Energy absorption is an important property of the interlayer material of the composite plate. In the tests, it was found that the polyurethane-foamed aluminum material had good energy absorption properties as it was able to dampen the explosive shock wave. This was an important finding in the tests. The energy absorption properties Q of a material are primarily related to the quantity of energy absorbed.

In a stress-strain curve, the area encircled by the starting stage to the compaction stage of the curve and the horizontal axis represents the energy absorbed by the buffer material within the strain variation range under the corresponding amount of stress. The size of the area reflects the energy absorption capability of the material under the relevant applied forces [16]. The energy absorption quantity Q can be defined as follows:

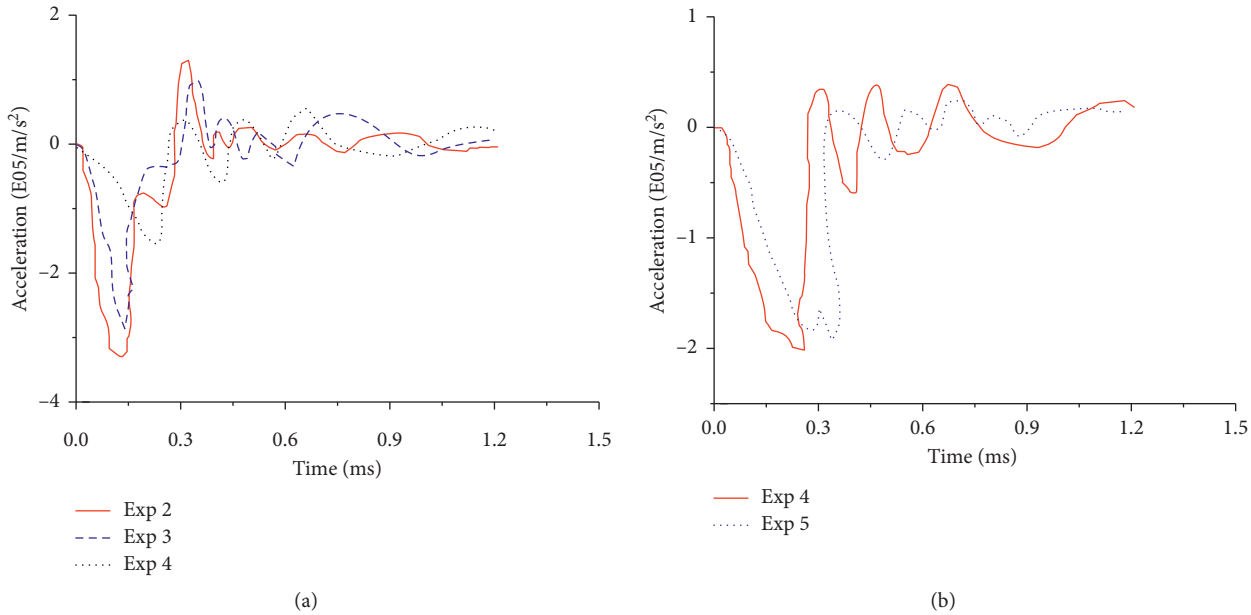

Figure 22: Test acceleration curves from the bottom of the bottom plates. (a) Tests 2, 3, and 4. (b) Tests 4 and 5.

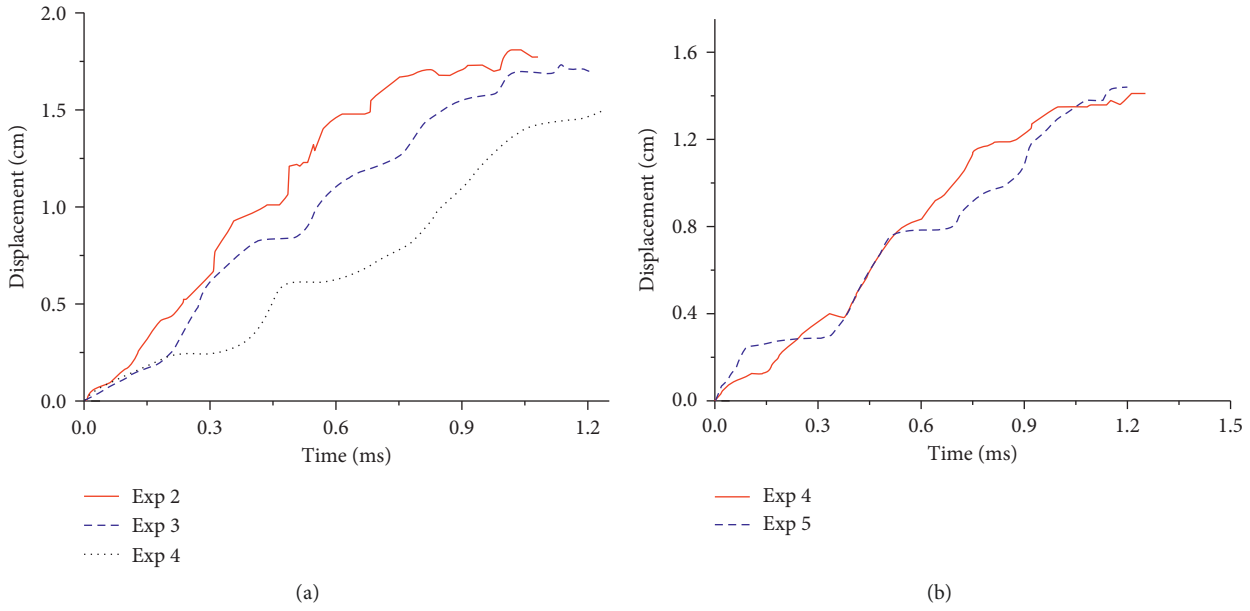

Figure 23: Bottom points of test displacement curves. (a) Tests 2, 3, and 4. (b) Tests 4 and 5.

$$Q = \int_0^{\varepsilon_i} \sigma \, d\varepsilon. \tag{1}$$

The result of Equation (1) is equivalent to the area below the dashed area of the curve shown in Figure 24.

The energy absorption efficiency is denoted as E and can be defined as follows:

$$E = \int_0^{\varepsilon_i} \frac{\sigma \, d\varepsilon}{\sigma_i} = \frac{Q}{\sigma_i}. \tag{2}$$

In Equation (2), the result after integration represents the ratio of the absorbed energy Q when the material is deformed to a certain strain under load and the corresponding stress represented by the energy absorption efficiency E of the material. When the energy absorption efficiency E reaches a maximum, this indicates that it has the best energy absorption capability under the corresponding strain and that the energy absorption was optimal.

According to the definition of the energy absorption quantity Q, the stress-strain curves of polyurethane-foamed

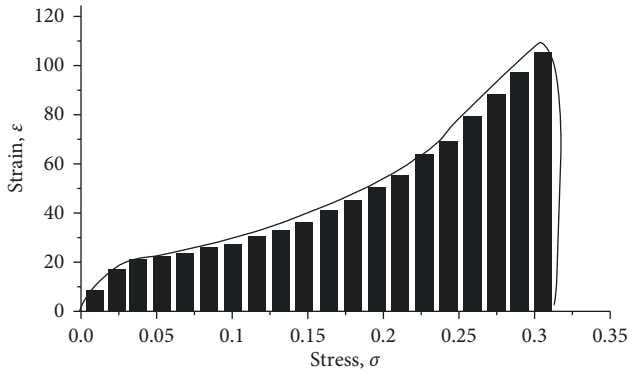

Figure 24: Materials energy absorption diagram.

aluminum and foamed aluminum were integrated (Figure 21) by means of Equation (1). Then, the energy at each strain stage derived from the integration was processed. The variable value of the horizontal axis was adjusted to obtain the strain-energy absorption quantity curve and the stress-energy absorption quantity curve (Figures 25 and 26). By comparing the energy absorption curves of the polyurethane-foamed aluminum and foamed aluminum, the energy absorption quantities of the two interlayer materials under explosive shock can be obtained. Ideally, the results will intuitively reflect the energy absorption capability of the two materials.

From Figure 25, it can be seen that the maximum energy absorbed by the polyurethane-foamed aluminum in the explosive destruction process in Test 3 was 8.58 MJ, which is larger than 7.78 MJ of energy absorbed by the foamed aluminum interlayer material. Also, it can be seen that as the strain increased, the slope of the energy absorption quantity curve of the polyurethane-foamed aluminum increased faster than that of the foamed aluminum. From Figure 26, it can be seen that, before the stress caused by the explosion reached 30 MPa, the energy-absorbing quantities of the two materials were similar. However, when the stress increased beyond 40 MPa, the polyurethane-foamed aluminum absorbed more energy.

According to the definition of the energy absorption efficiency E, when a material has the maximum energy absorption efficiency, this proves that the material is ideal and has the best energy absorption status. From the test data, the energy absorption efficiency-stress curves and the energy absorption efficiency-strain curves of the polyurethane-foamed aluminum and foamed aluminum were obtained, as shown in Figures 27 and 28. From Figure 27, it can be seen that as the strain grew, the slope of the energy absorption efficiency curve of the polyurethane-foamed aluminum increased faster than that of the foamed aluminum. For this reason, when the material deformation was large, the polyurethane-foamed aluminum material had a higher energy absorption capability. From Figure 28, it can be seen that foamed aluminum had the best energy-absorbing status when the stress was in the range of 25 to 33 MPa, while the polyurethane-foamed aluminum achieved an optimal state within a stress range of 33 to 40 MPa.

By analyzing the energy absorption quantities and efficiencies of polyurethane-foamed aluminum and foamed

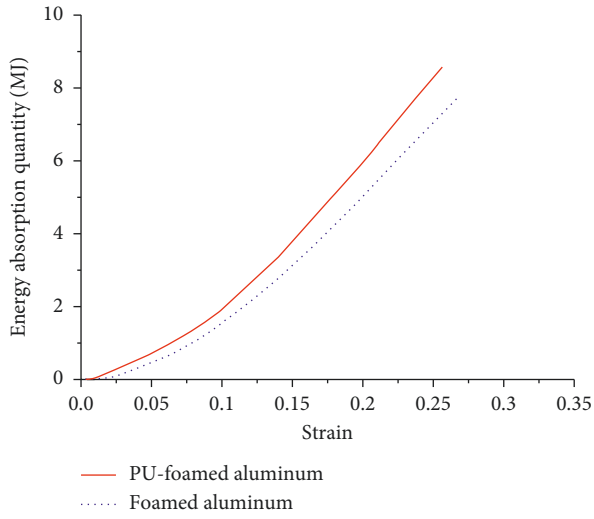

Figure 25: Energy absorption-strain curve.

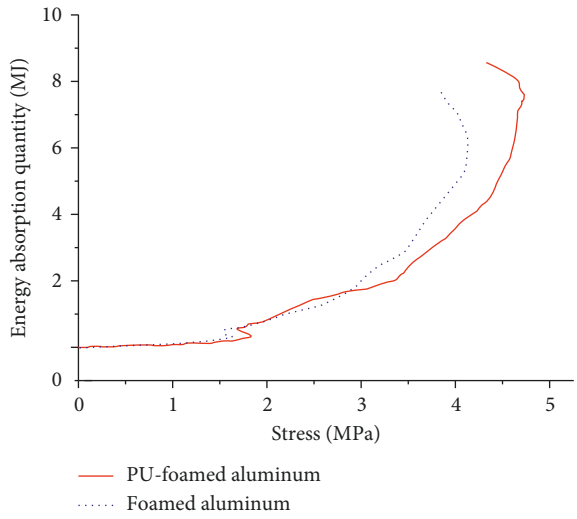

Figure 26: Energy absorption-stress curve.

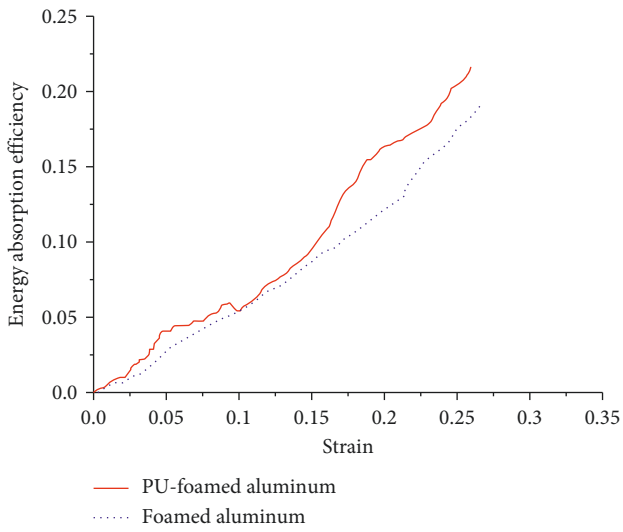

Figure 27: Energy absorption efficiency-strain curve.

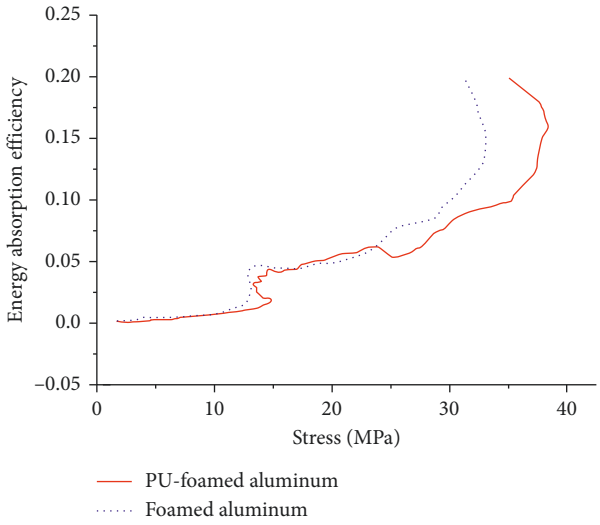

Figure 28: Energy absorption efficiency-stress curve.

aluminum, it was concluded that polyurethane-foamed aluminum had better energy absorption capability than foamed aluminum when the stress was higher than 33 MPa. In the tests, the polyurethane-foamed aluminum interlayer absorbed more energy than the foamed aluminum interlayer.

5. Conclusions

By analyzing the results of the explosions and tests, it was found that the polyurethane-foamed aluminum had better absorption for an explosive shock wave than the foamed aluminum, and the thickness of the polyurethane-foamed aluminum had a remarkable impact on the energy absorption and explosion resistance effects. However, when the polyurethane-foamed aluminum plate was divided into two layers with the same overall thickness, the performance of the split layers was not significantly better. This demonstrated that the overall structure of the layers did not have a significant impact.

It was seen from analyzing the energy absorption capability that the polyurethane-foamed aluminum had obvious advantages in terms of the energy absorption quantity and efficiency. Under the same explosive environment, the maximum energy absorbed by the polyurethane-foamed aluminum in the explosive destruction process was 8.58 MJ, while that by the foamed aluminum interlayer material was 7.78 MJ.

Data Availability

The data used to support the findings of this study are available from the corresponding author upon request.

Conflicts of Interest

The authors declare that they have no conflicts of interest.

Acknowledgments

The authors express their thanks to the National Natural Science Foundation of China (grant numbers 51478462 and 51508565).

References

[1] H. B. Lu, Y. Liu, B.-K. Zhou et al., "Experimental study on the explosion resistance performance of high-strength RC slabs," *Journal of Wuhan University of Technology*, vol. 34, no. 10, pp. 91–95, 2012.

[2] C. Zhai, L. Chen, H. Xiang, and Q. Fang, "Experimental and numerical investigation into RC beams subjected to blast after exposure to fire," *International Journal of Impact Engineering*, vol. 97, pp. 29–45, 2016.

[3] Z.-H. Zong, B. Tang, C. Gao, L. Liu, M.-H. Li, and S.-J. Yuan, "Experiment on blast-resistance performance of reinforced concrete piers," *China Journal of Highway and Transport*, vol. 30, no. 9, pp. 51–60, 2017.

[4] L. Chen, Q. Fang, X. Jiang, Z. Ruan, and J. Hong, "Combined effects of high temperature and high strain rate on normal weight concrete," *International Journal of Impact Engineering*, vol. 86, pp. 40–56, 2015.

[5] X. Yu, L. Chen, Q. Fang, Z. Ruan, J. Hong, and H. Xiang, "A concrete constitutive model considering coupled effects of high temperature and high strain rate," *International Journal of Impact Engineering*, vol. 101, pp. 66–77, 2017.

[6] J. Shen, G. Lu, Z. Wang, and L. Zhao, "Experiments on curved sandwich panels under blast loading," *International Journal of Impact Engineering*, vol. 37, no. 9, pp. 960–970, 2010.

[7] R. P. Merrett, G. S. Langdon, and M. D. Theobald, "The blast and impact loading of aluminum foam," *Materials and Design*, vol. 44, no. 1, pp. 311–319, 2012.

[8] N.-R. Yun, D.-H. Shin, S.-W. Ji, and C.-S. Shim, "Experiments on blast protective systems using aluminum foam panels," *KSCE Journal of Civil Engineering*, vol. 18, no. 7, pp. 2153–2161, 2014.

[9] G.-Y. Zeng, F. D Nie, L. Liu et al., "In-situ crystallization coating HMX by polyurethane," *Chinese Journal of Energetic Materials*, vol. 19, no. 2, pp. 138–141, 2011.

[10] C.-C. Zhu, H.-Y. Weng, G.-H. Lv et al., "The Latest development status of polyurethane industry at home and abroad," *Chemical Propellants & Polymeric Materials*, vol. 5, pp. 1–20, 2012.

[11] D.-M. Wang, S.-L. Xia, L.-Q. Zhang et al., "Research progress in the preparation methods of polyurethane/nano-composite materials," *Polymer Bulletin*, vol. 3, pp. 65–72, 2011.

[12] W. Zhang, M. Qi, Z. Zhao et al., "Preparation and mechanical property analysis of aluminum foam-polyurethane composites," *Packing Engineering*, vol. 38, no. 21, pp. 35–40, 2017.

[13] W.-H. Xie, H.-T. Du, and S.-C. Li, "Comparative study of energy absorption performance for open cell aluminum and polyurethane foam aluminum," *Journal of Shenyang Jianzhu University (Natural Science)*, vol. 2, pp. 307–311, 2011.

[14] W.-H. Xie, H.-T. Du, and S.-C. Li, "Experimental study on dynamic mechanical performance of polyurethane aluminum foams composites," *Acta Materiae Compositae Sinica*, vol. 3, pp. 103–108, 2011.

[15] Y. Zhang, L. Chen, R.-J. Chen et al., "Dynamic mechanical property experiment and constitutive model establishment of polyurethane foam aluminum," *Explosion and Shock Waves*, vol. 3, pp. 373–378, 2014.

[16] S.-B. Sui, J.-G. Kang, and J.-H. Sun, "Energy absorption and vibration reduction performance of aluminum foam under fuel-air explosion loading," *Blasting*, vol. 2, pp. 30–34, 2011.